Water vapor and the hydrological cycle

Time and zonal mean *saturation* specific humidity

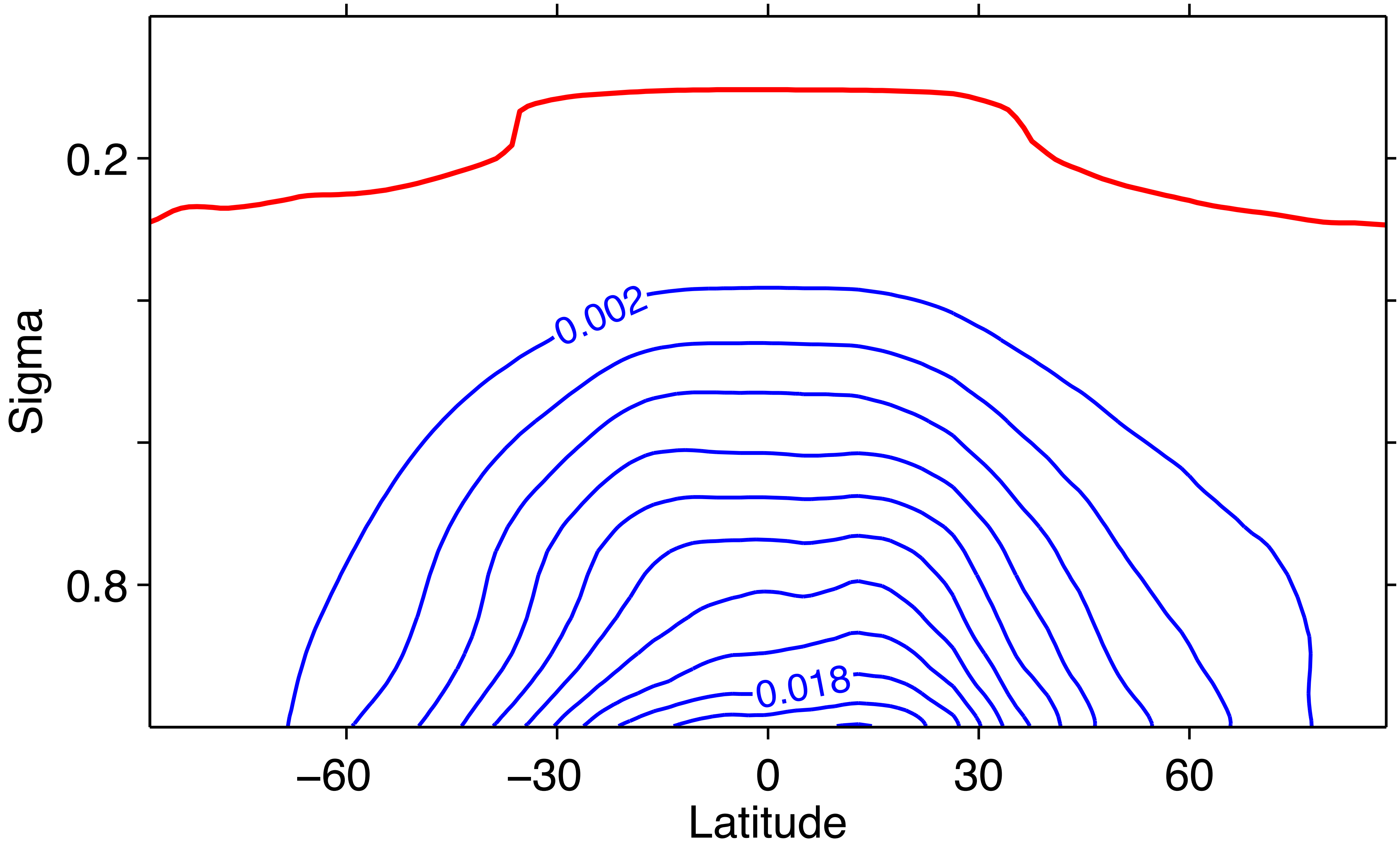

ERA40, 1980-2001

Fig. 1

Time and zonal mean specific humidity

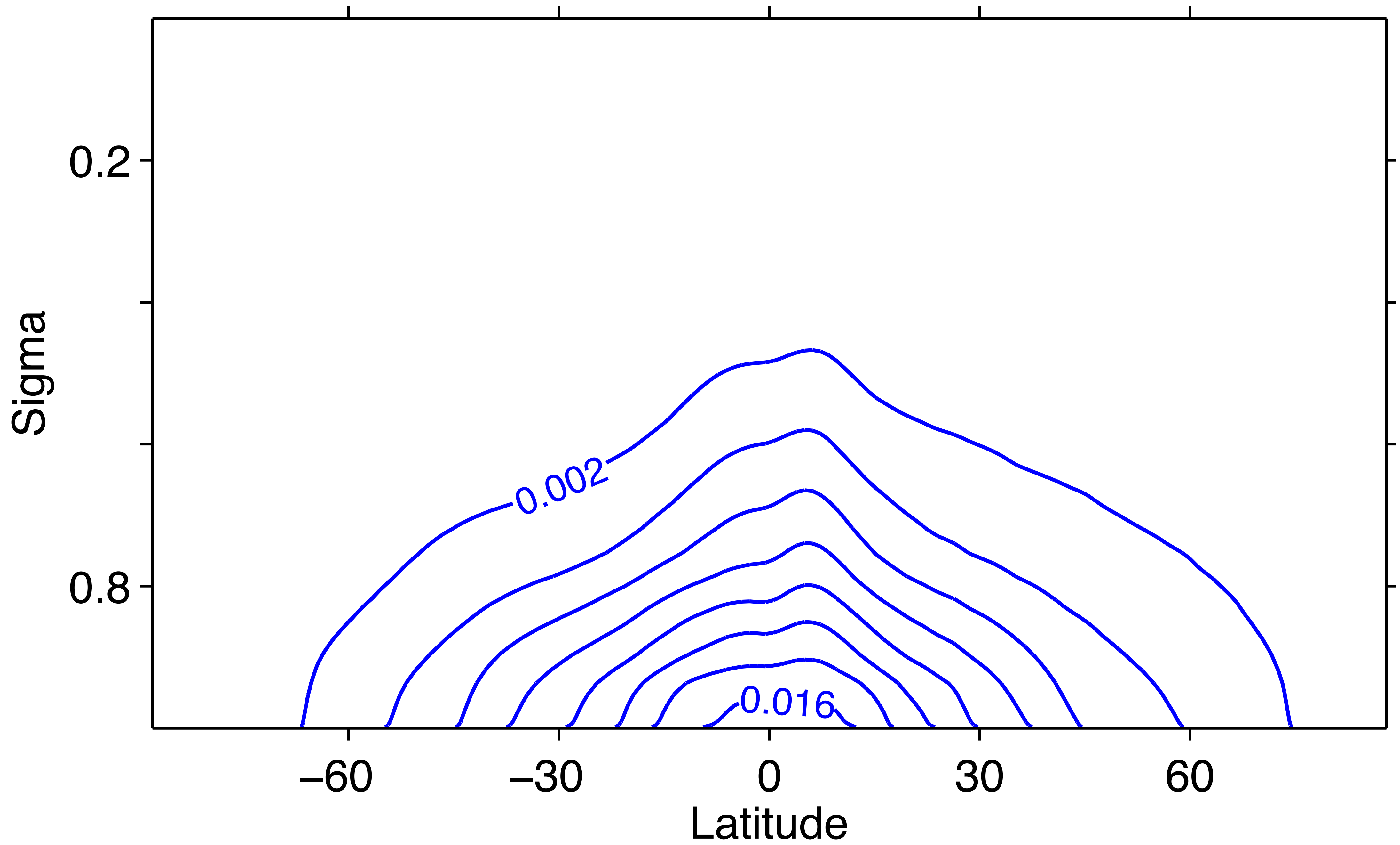

ERA40, 1980-2001

Fig. 2

Time and zonal mean *relative* humidity: seasons

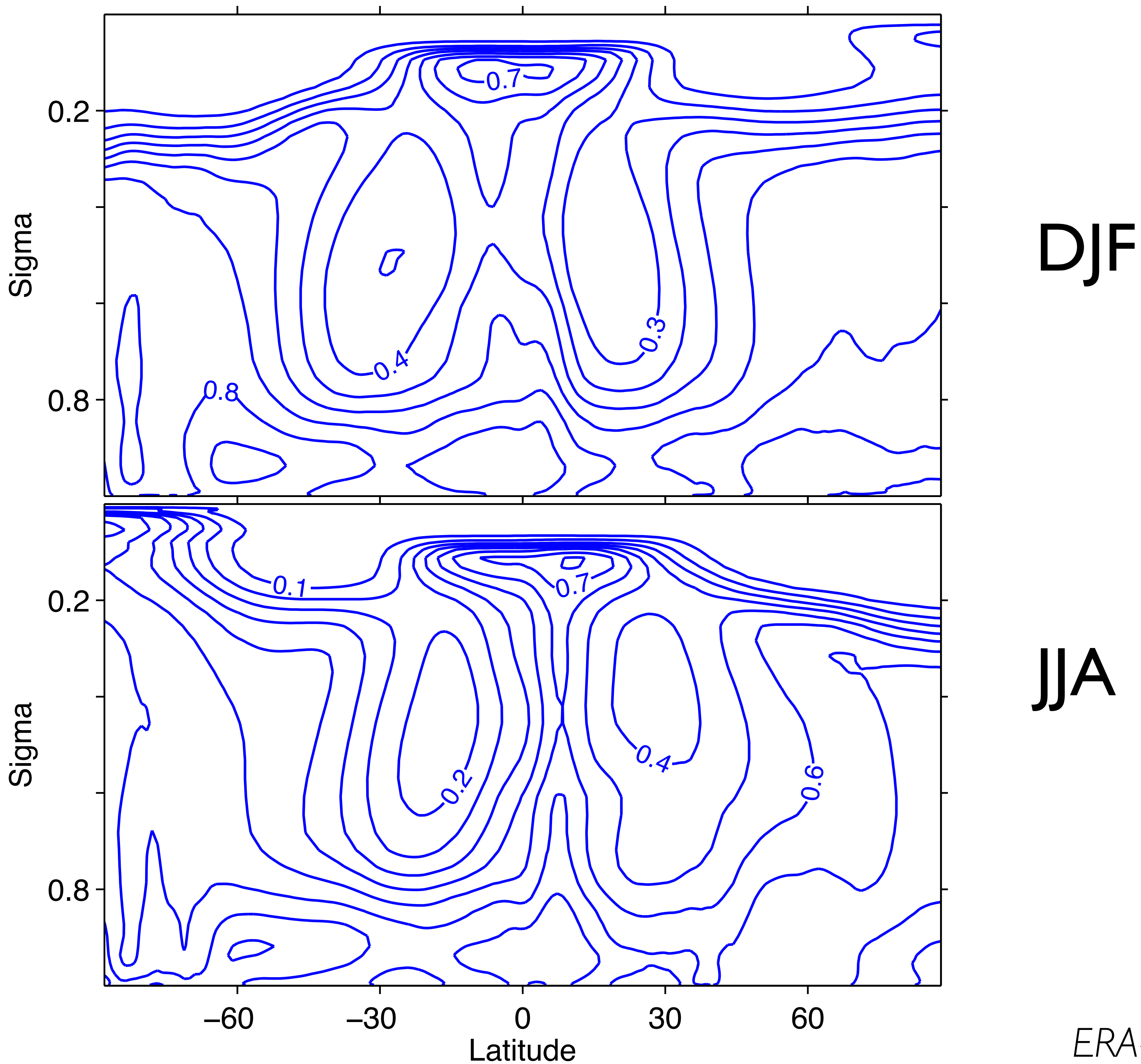

ERA40, 1980-2001

Fig. 3

Time mean relative humidity at 500hPa

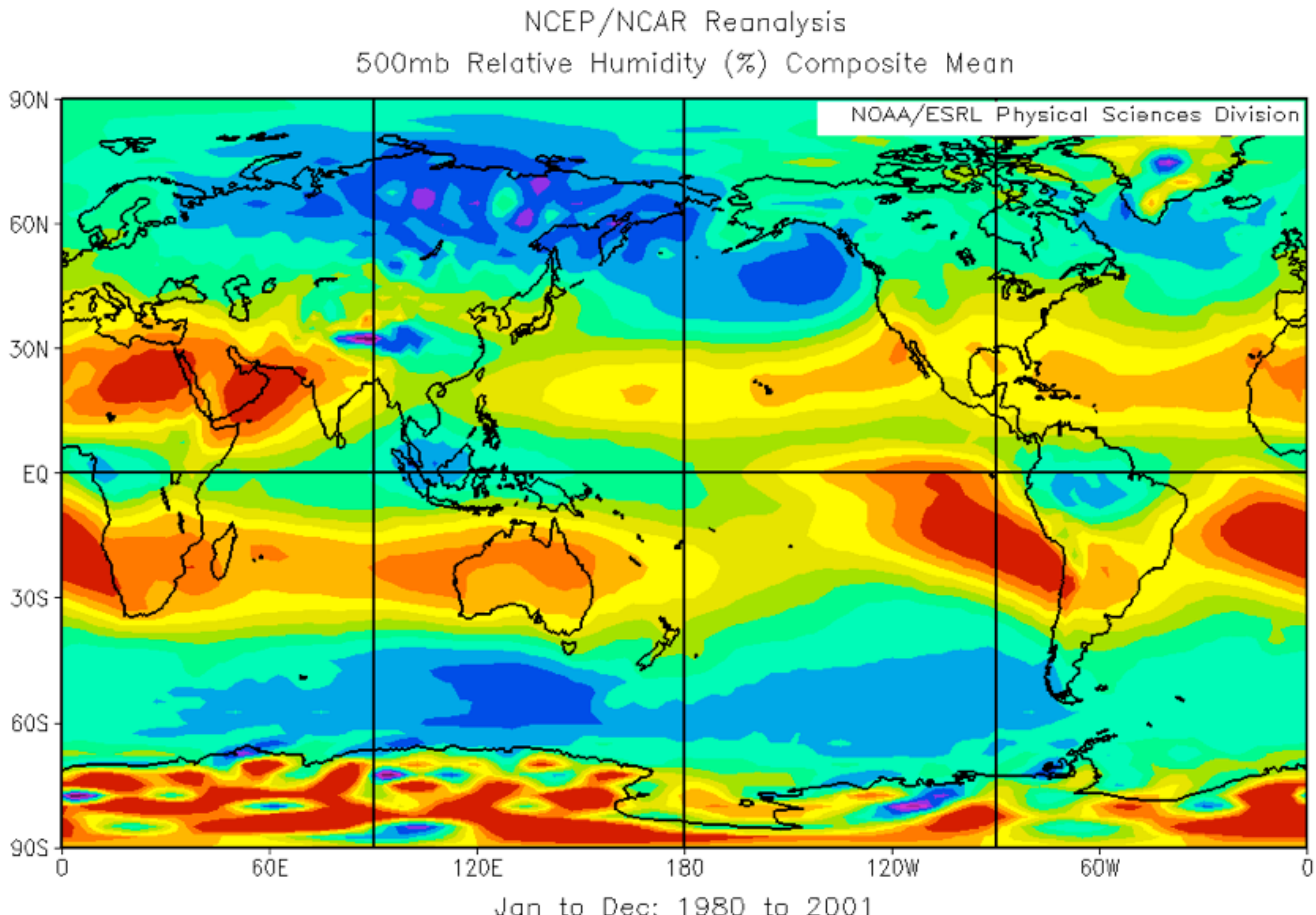

Fig. 4

CDC interactive plotting

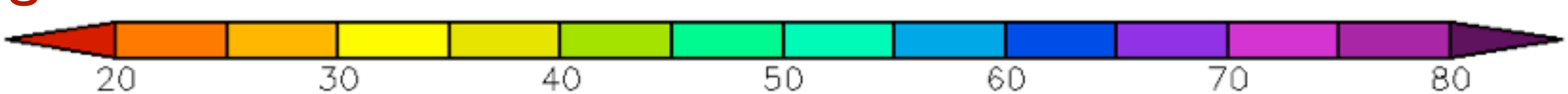

Vertical-mean zonal flux of water vapor (m/s g/kg)

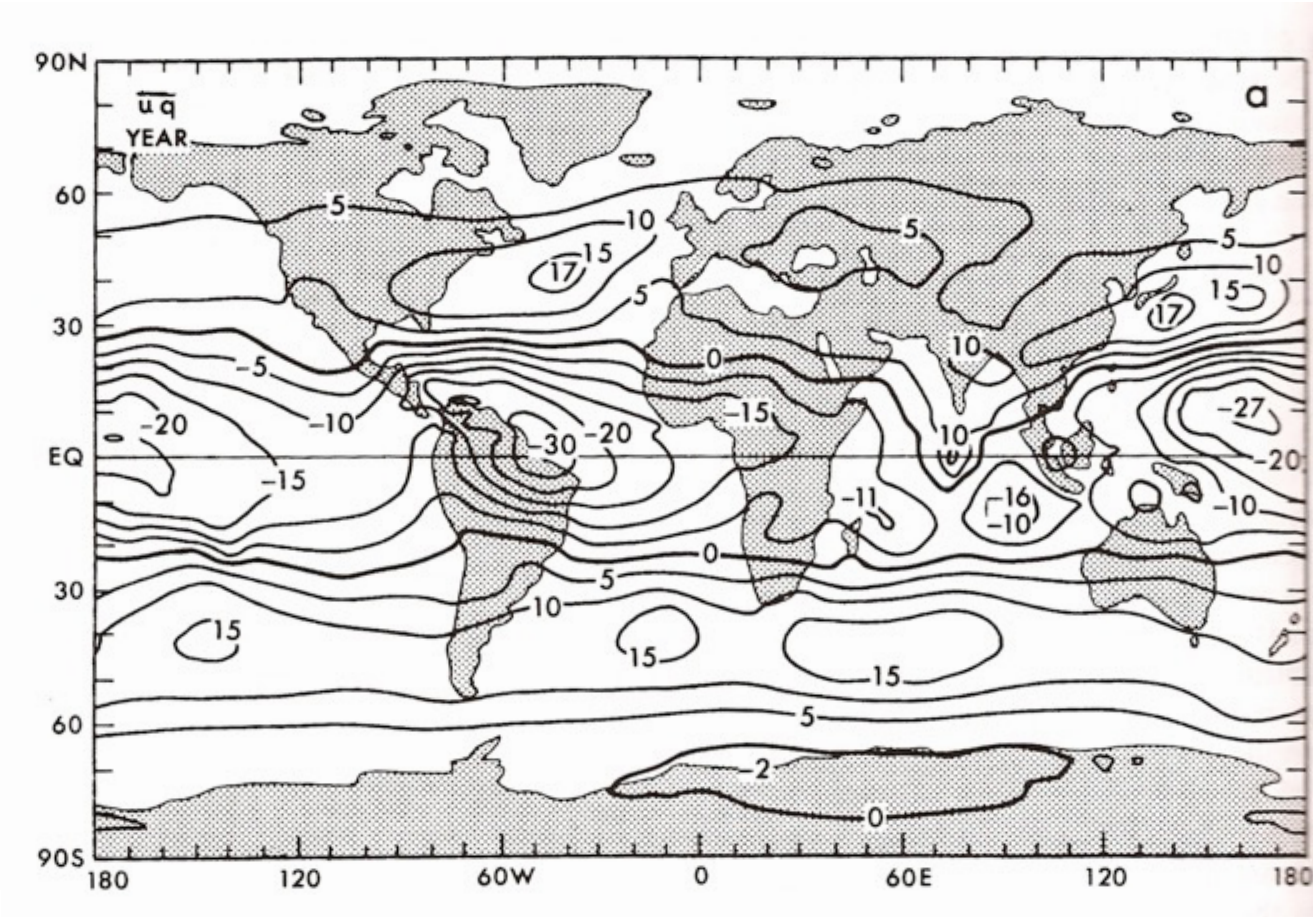

Fig. 5

Peixoto and Oort, Fig 12.7

Vertical-mean *transient* zonal flux of water vapor (m/s g/kg)

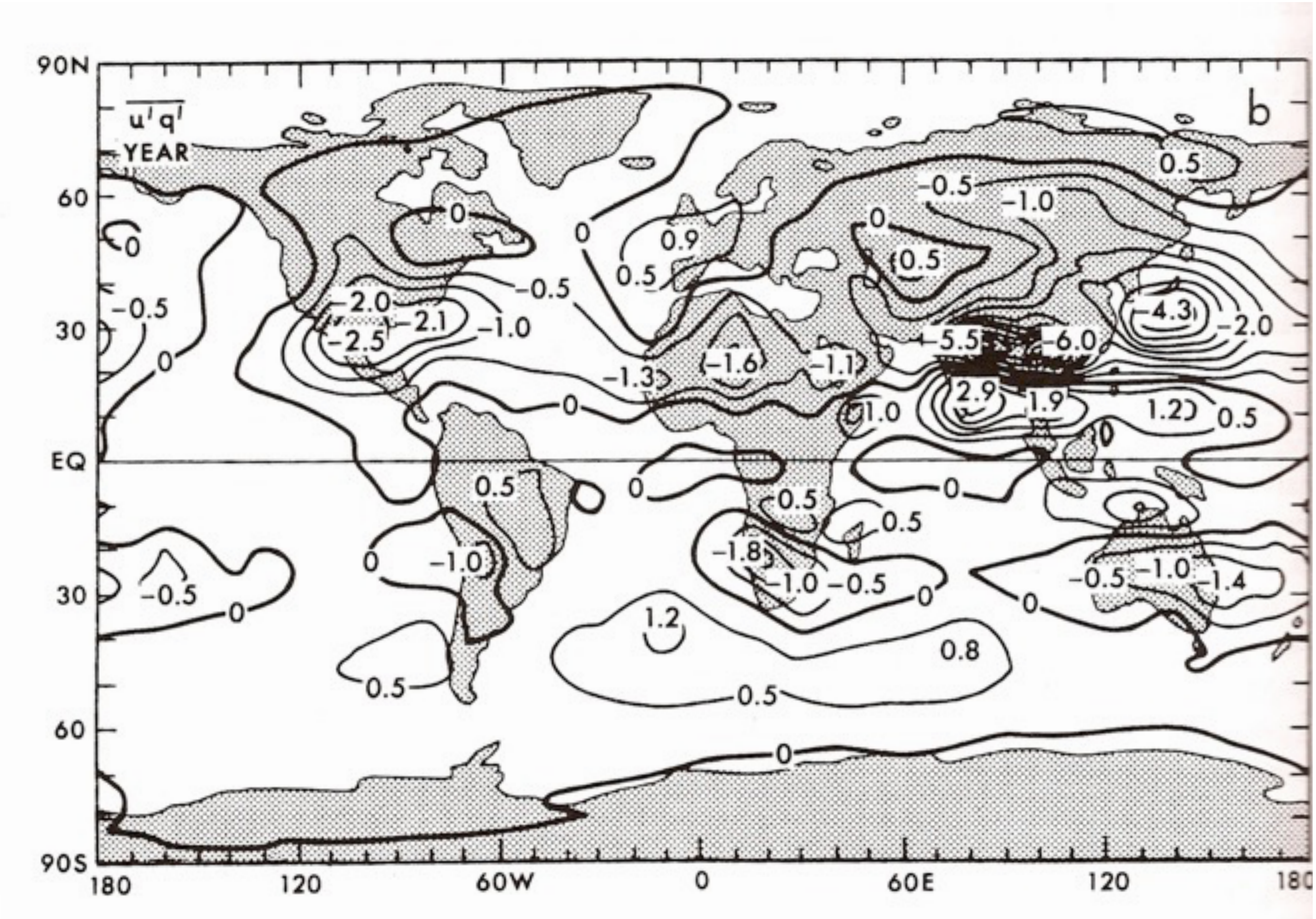

Fig. 6

Peixoto and Oort, Fig 12.7

Vertical-mean meridional flux of water vapor (m/s g/kg)

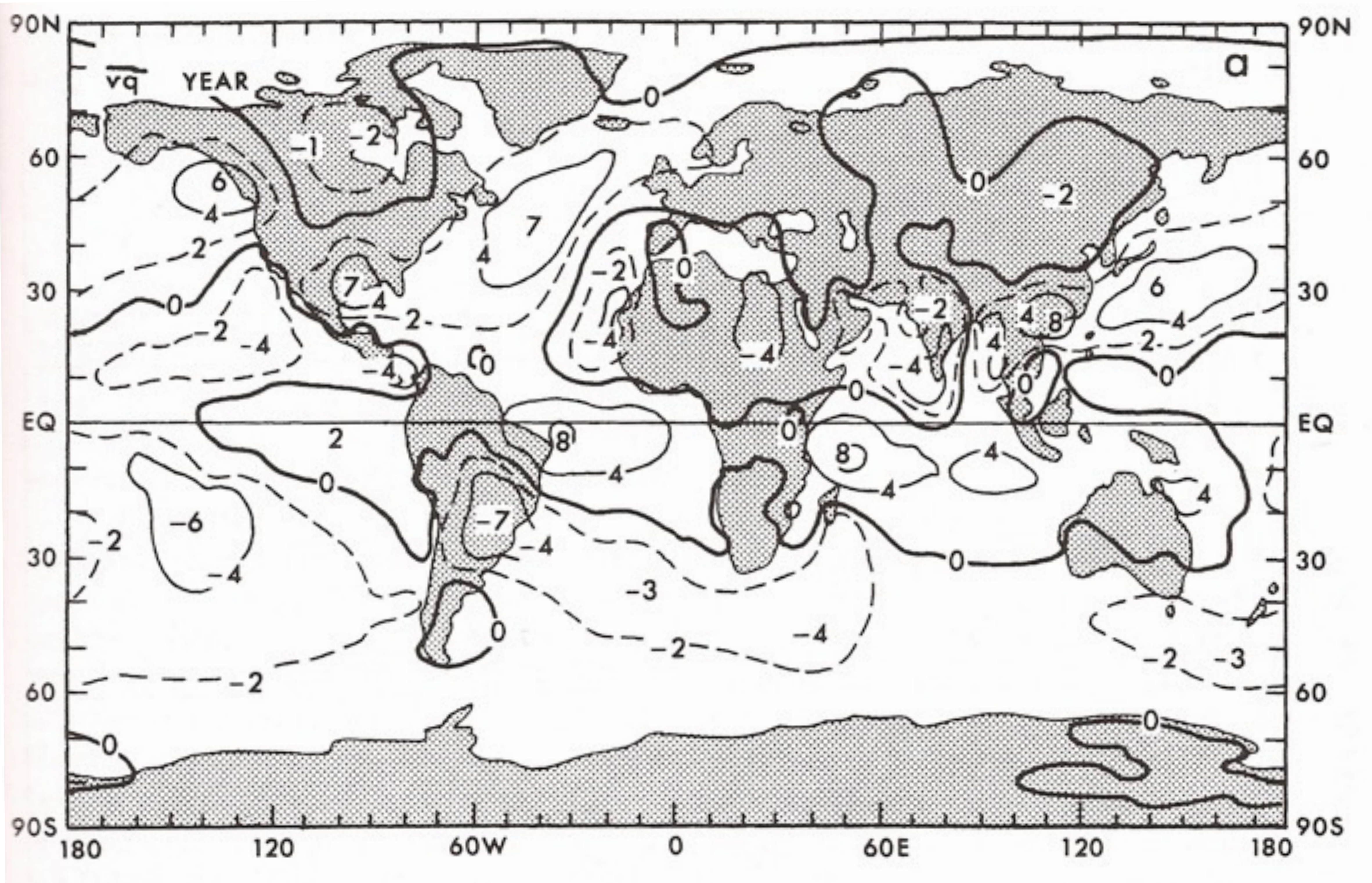

Fig. 7

Peixoto and Oort, Fig 12.10

Meridional flux of water vapor (m/s g/kg)

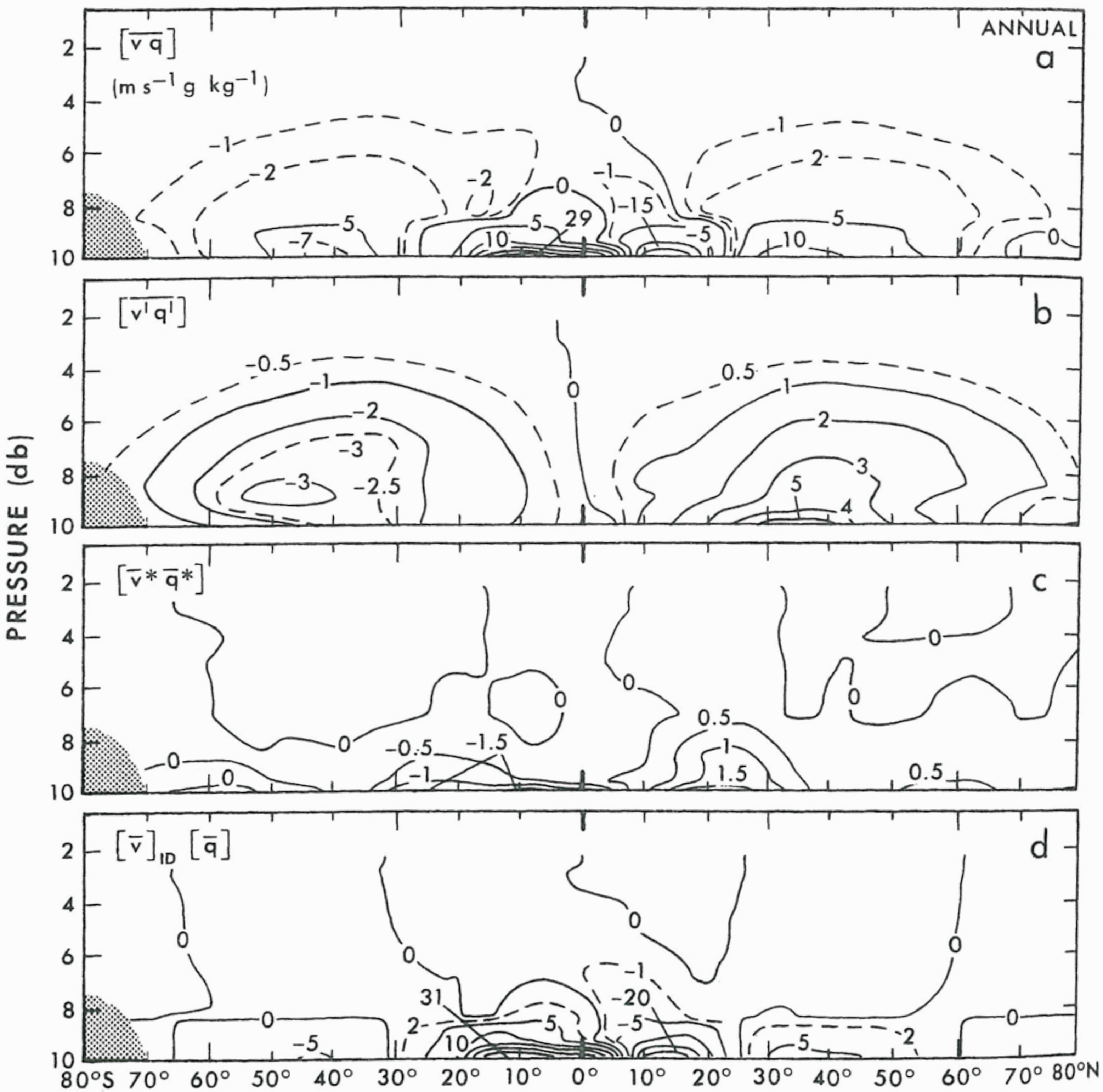

Total

Transient

Stationary

Mean

Fig. 8

FIGURE 12.11. Zonal-mean cross sections of the northward transport of water vapor by all motions (a), transient eddies (b), stationary eddies (c), and mean meridional circulations (d) in m s^{-1} g kg^{-1} for annual-mean conditions.

Peixoto and Oort, Fig 12.11

Vertical eddy flux of water vapor (10^{-10}/s)

sigma coordinate vertical velocity, both transient and stationary eddies

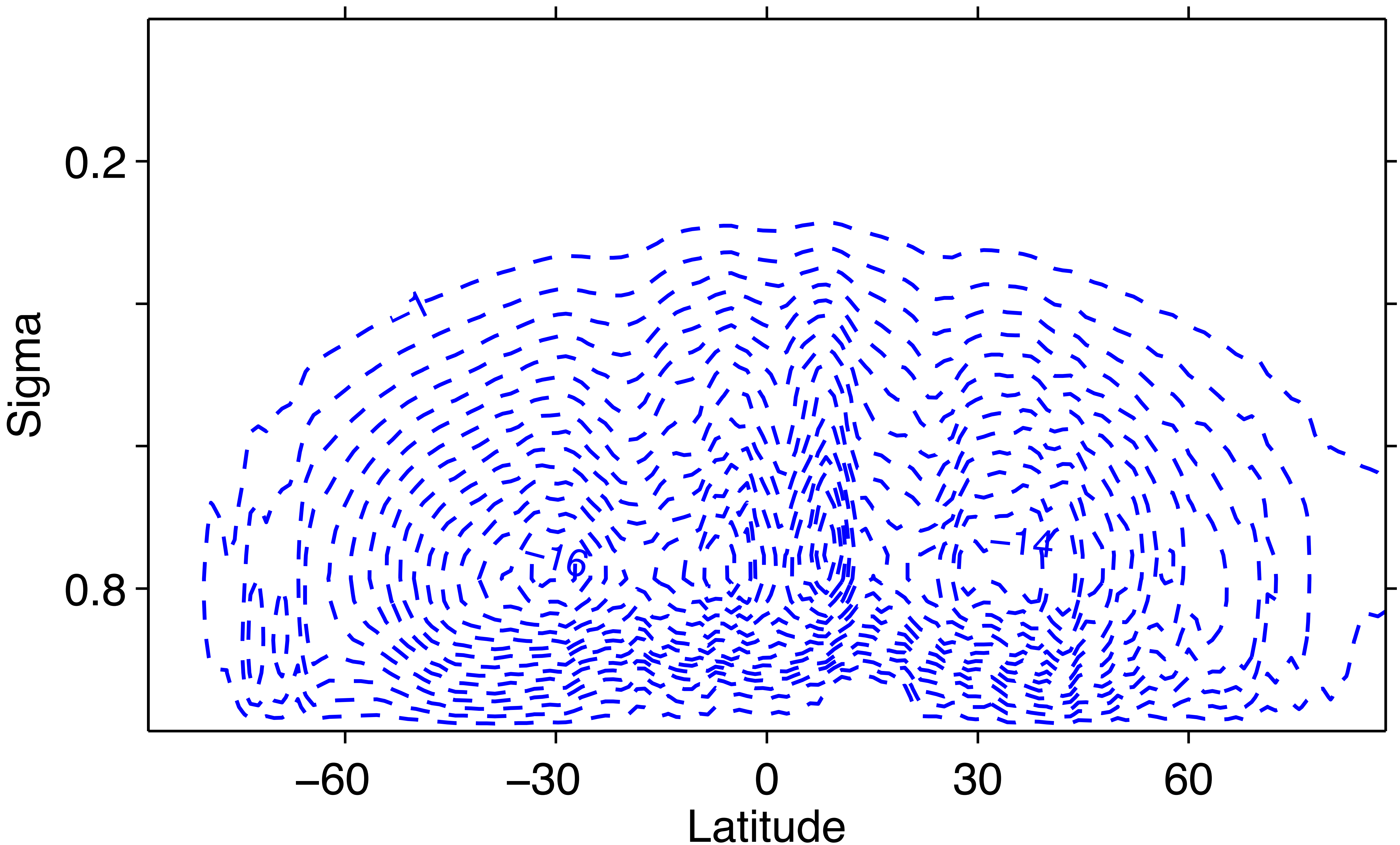

Fig. 9

ERA40, 1980-2001

Water vapor+condensate streamfunction

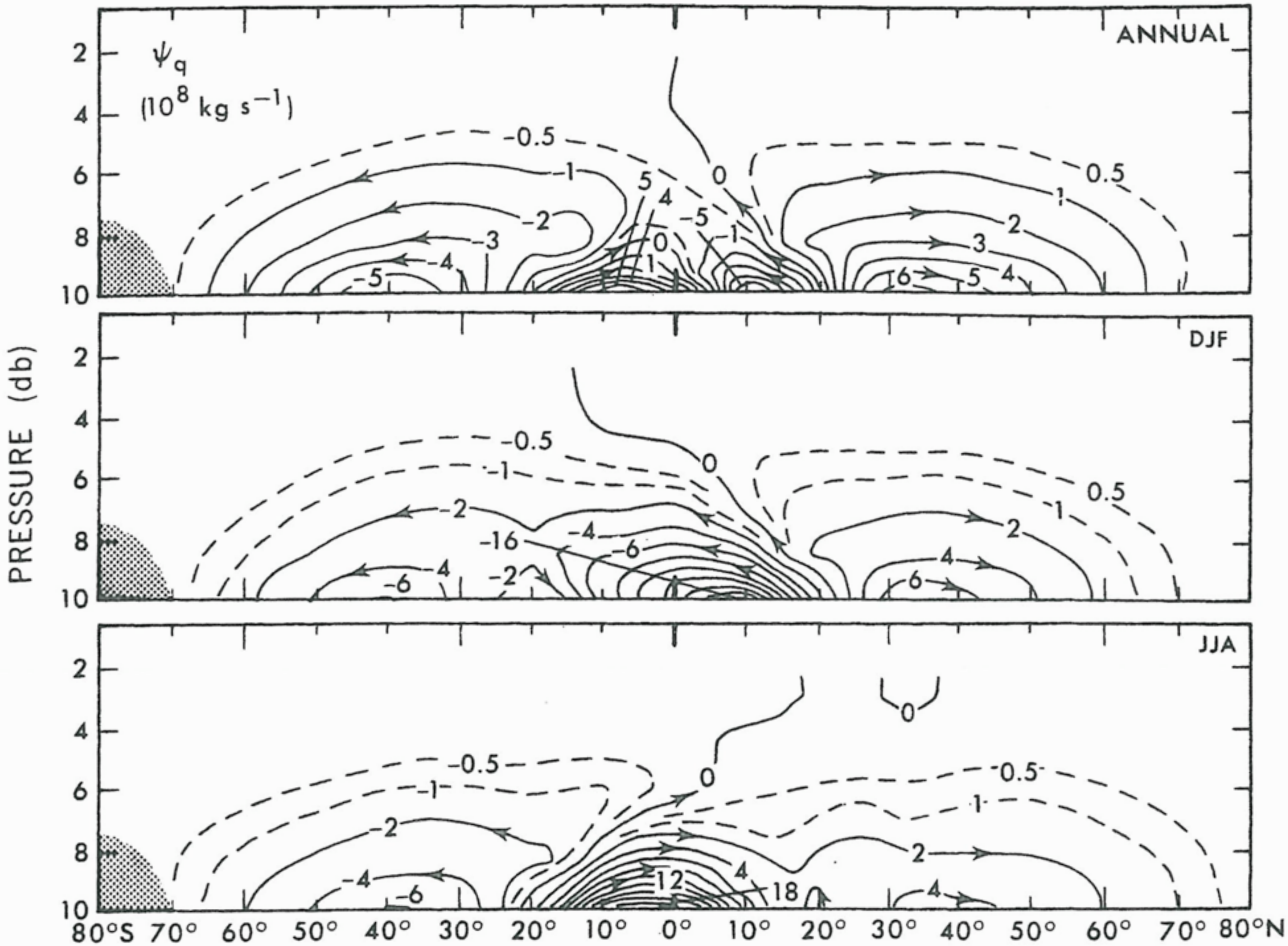

FIGURE 12.18. Streamlines of the zonal-mean transport of water vapor for annual, DJF, and JJA mean conditions in 10^8 kg s^{-1} (from Peixoto and Oort, 1983).

Fig. 10

Peixoto and Oort, Fig 12.18

E-P (mm/day)

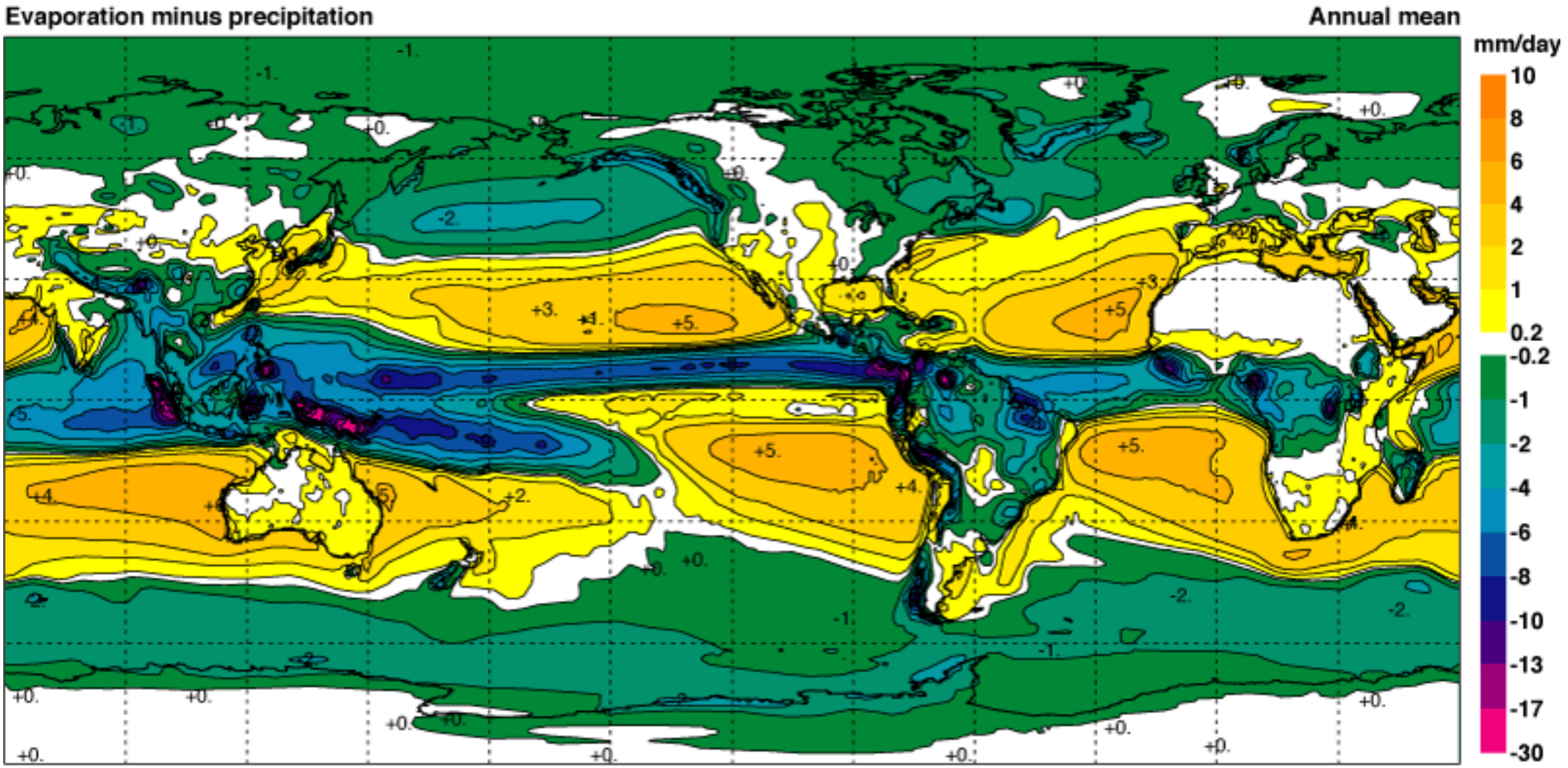

Fig. 11

ERA40 atlas

Zonal-mean E-P (0.01 m/yr)

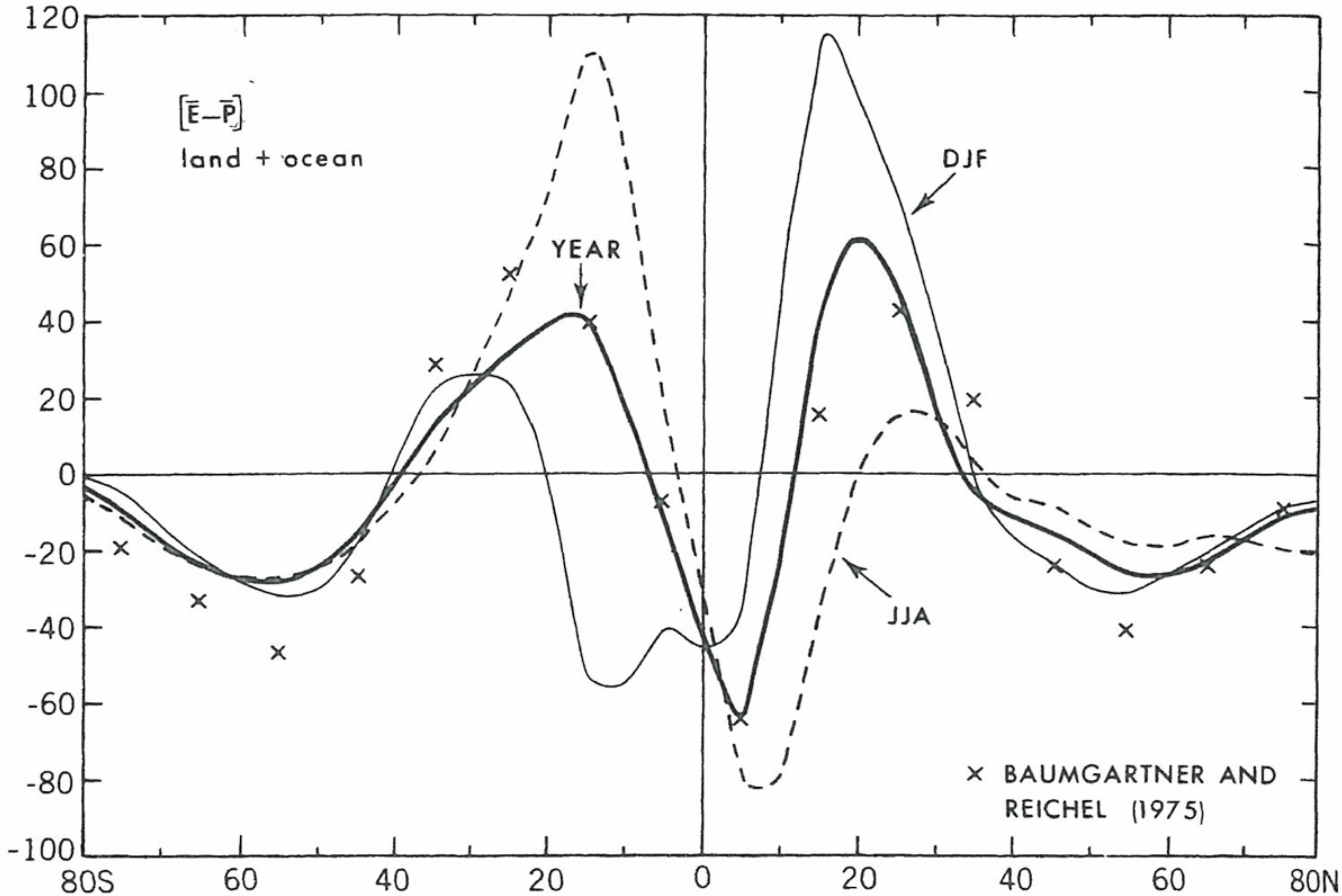

FIGURE 12.16. Meridional profiles of the zonal-mean divergence of the total water vapor transport [div **Q**] ≈ [$E - P$] in 0.01 m yr^{-1} for annual, DJF, and JJA mean conditions. Some annual-mean estimates of $E - P$ by Baumgartner and Reichel (1975) are added for comparison (see also Table 7.1).

Peixoto and Oort, Fig 12.16

Fig. 12

Schematic of water vapor transports

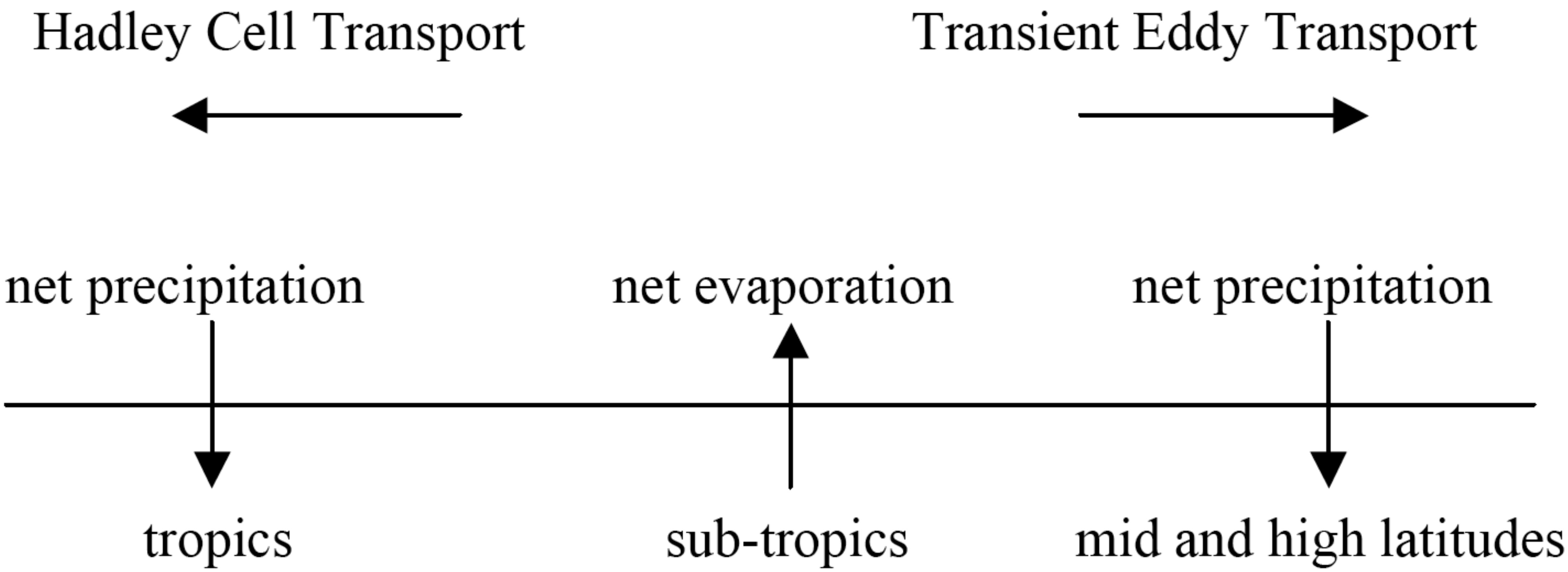

Fig. 13

MIT OCW

DJF Water vapor flux (each barb 2 m s^{-1} g kg^{-1}) and some streamlines

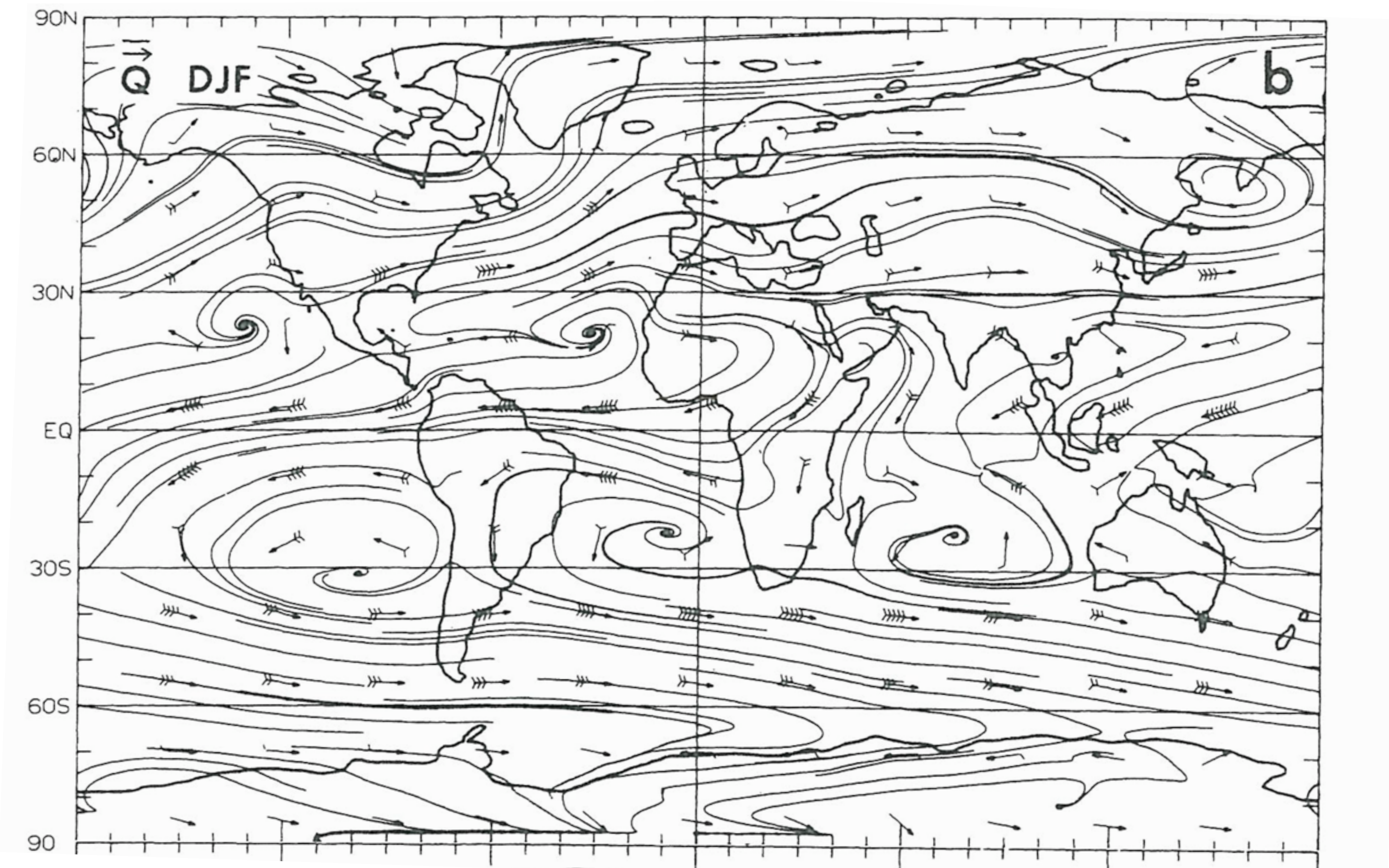

Fig. 14

Peixoto and Oort, Fig 12.17b

Estimates of evaporation and precipitation rates

Estimation of precipitation

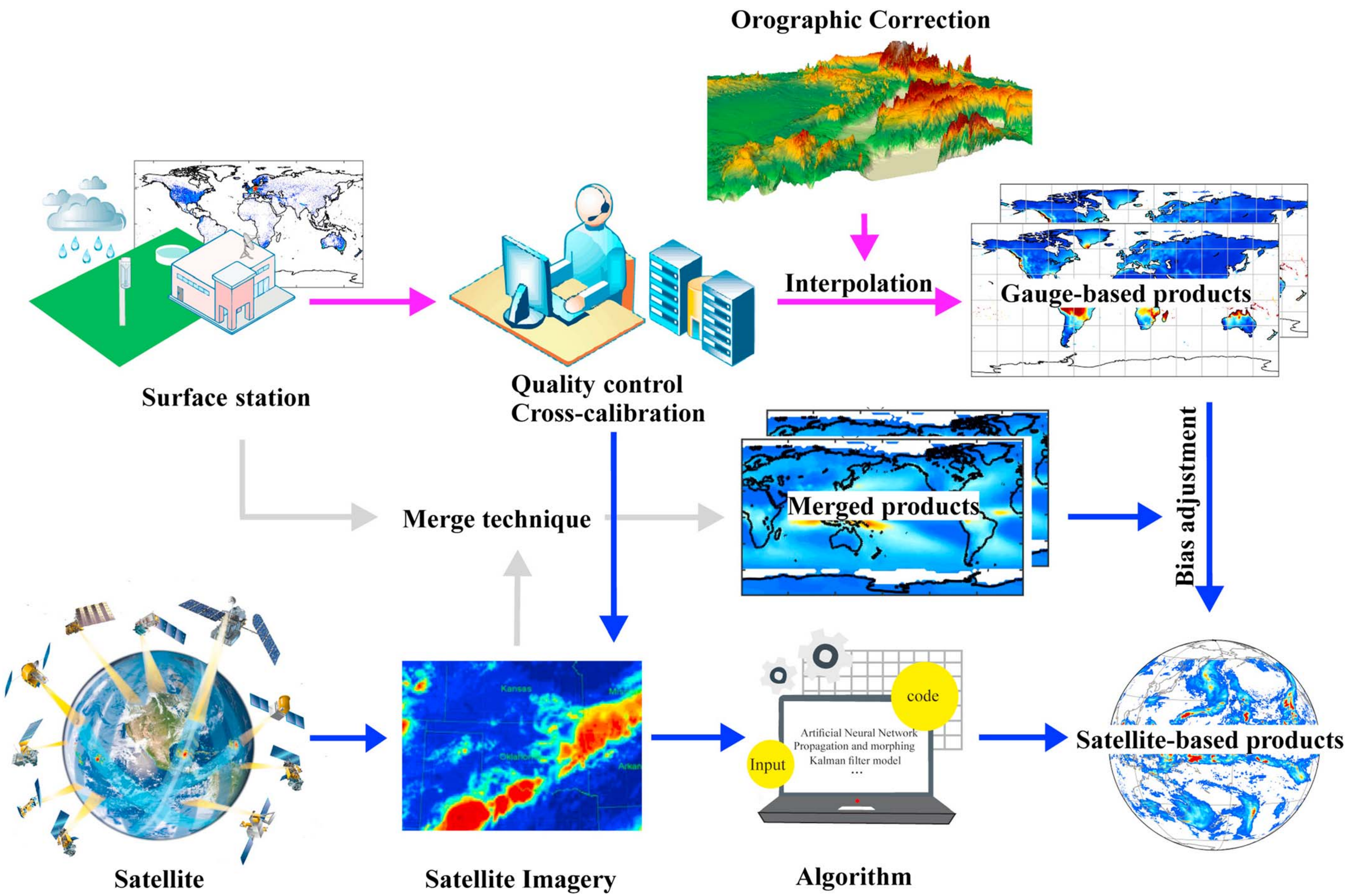

Figure 4. Flowchart for the precipitation products. The images for satellite adapted from Hou et al. (2014).

Fig. 15

Sun, Reviews of Geophysics, 2018

GPCP: long-term mean precipitation

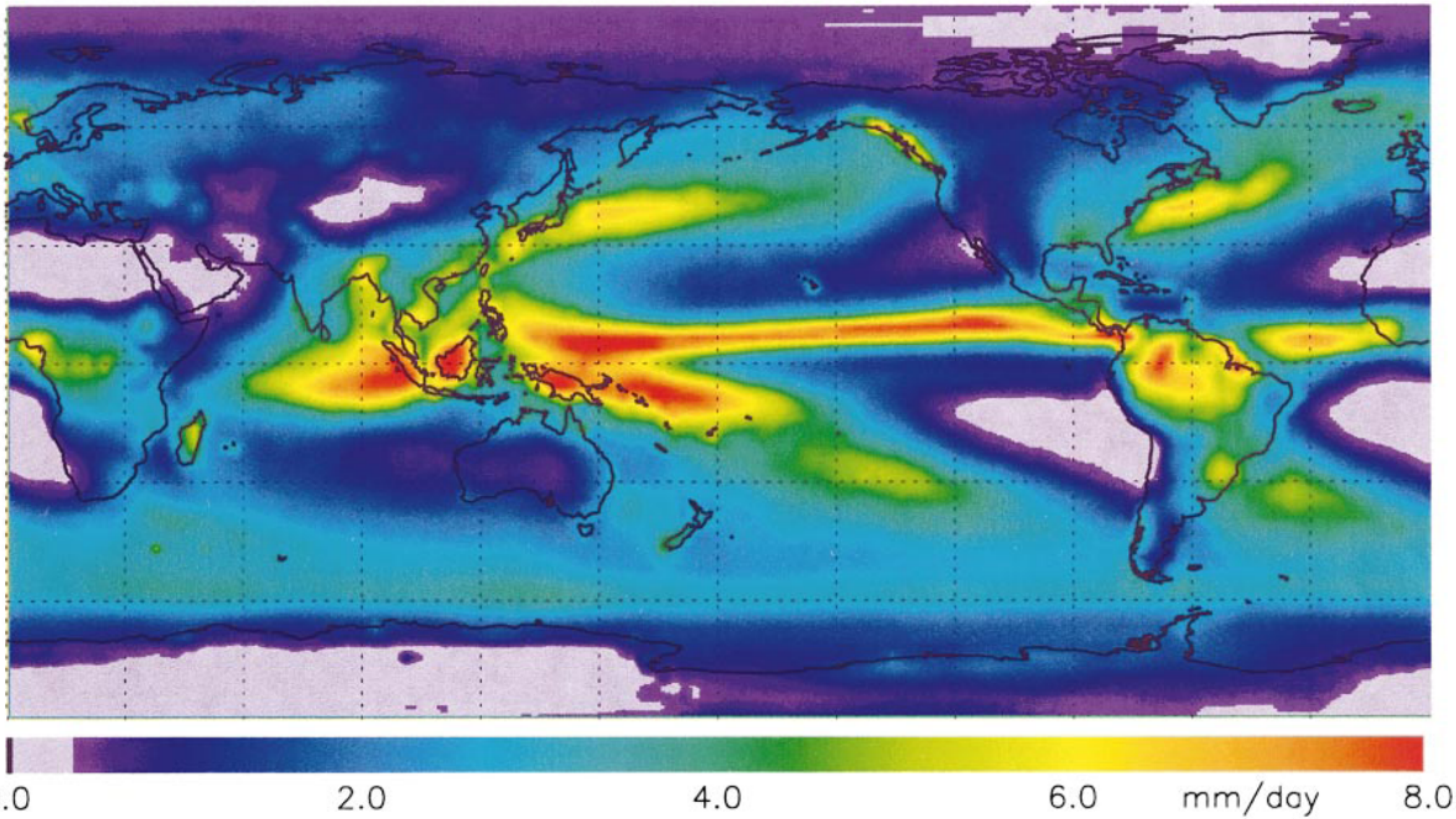

FIG. 4. The 23-yr (1979–2001) annual mean precipitation (mm day^{-1}).

Fig. 16

Adler, J. Hydrometeor., 2003

GPCP Algorithm

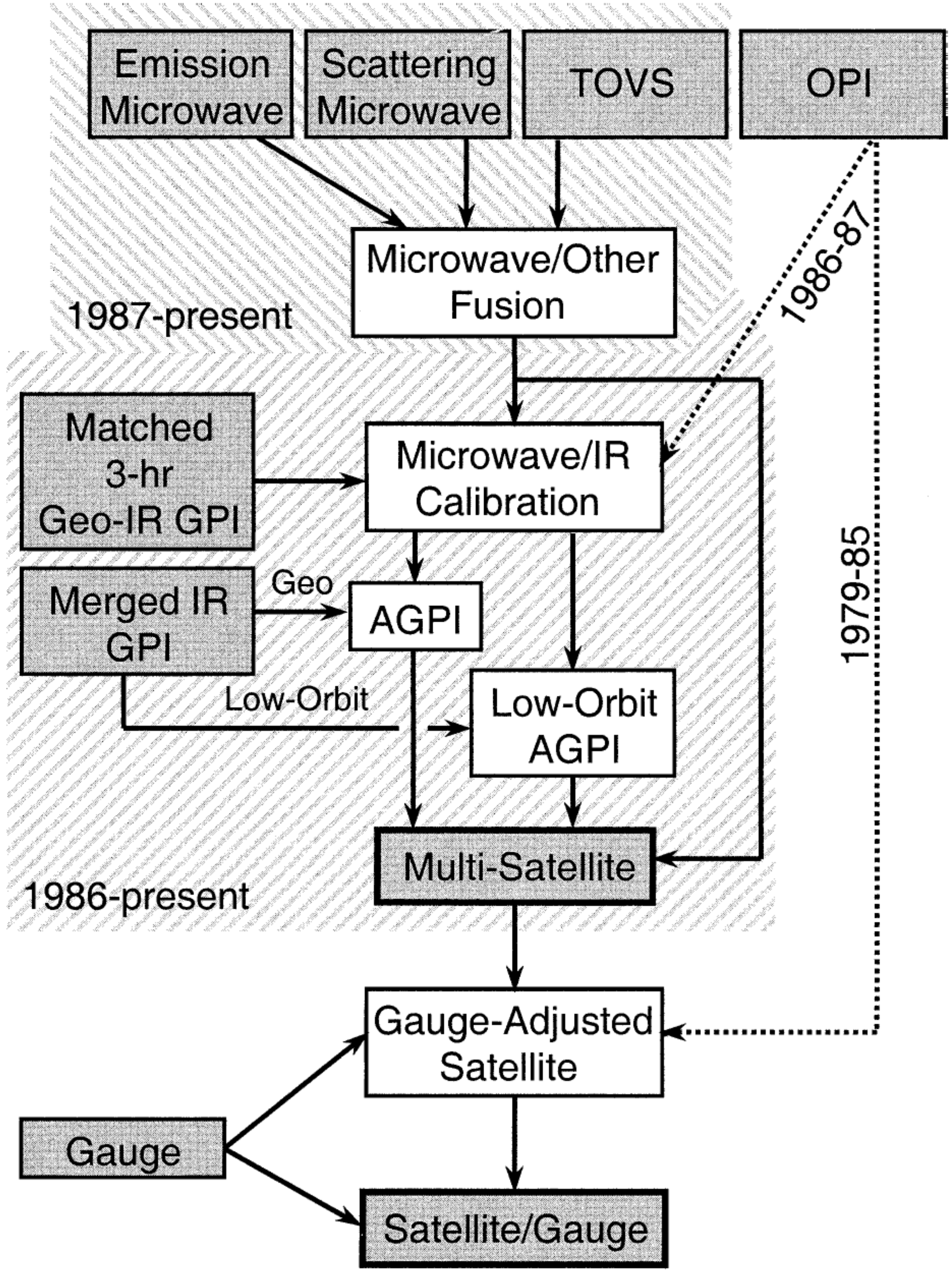

FIG. 1. Block diagram of the Version-2 satellite–gauge (SG) precipitation combination technique. Shaded boxes with thin borders are input datasets, shaded boxes with thick borders are output datasets produced in the SG, and unshaded boxes are intermediate datasets produced in the SG. Arrows show data flow. Hatched background and dotted arrows indicate the years for which various parts of the computation are done, as described in the text.

Fig. 17

Adler, J. Hydrometeor., 2003

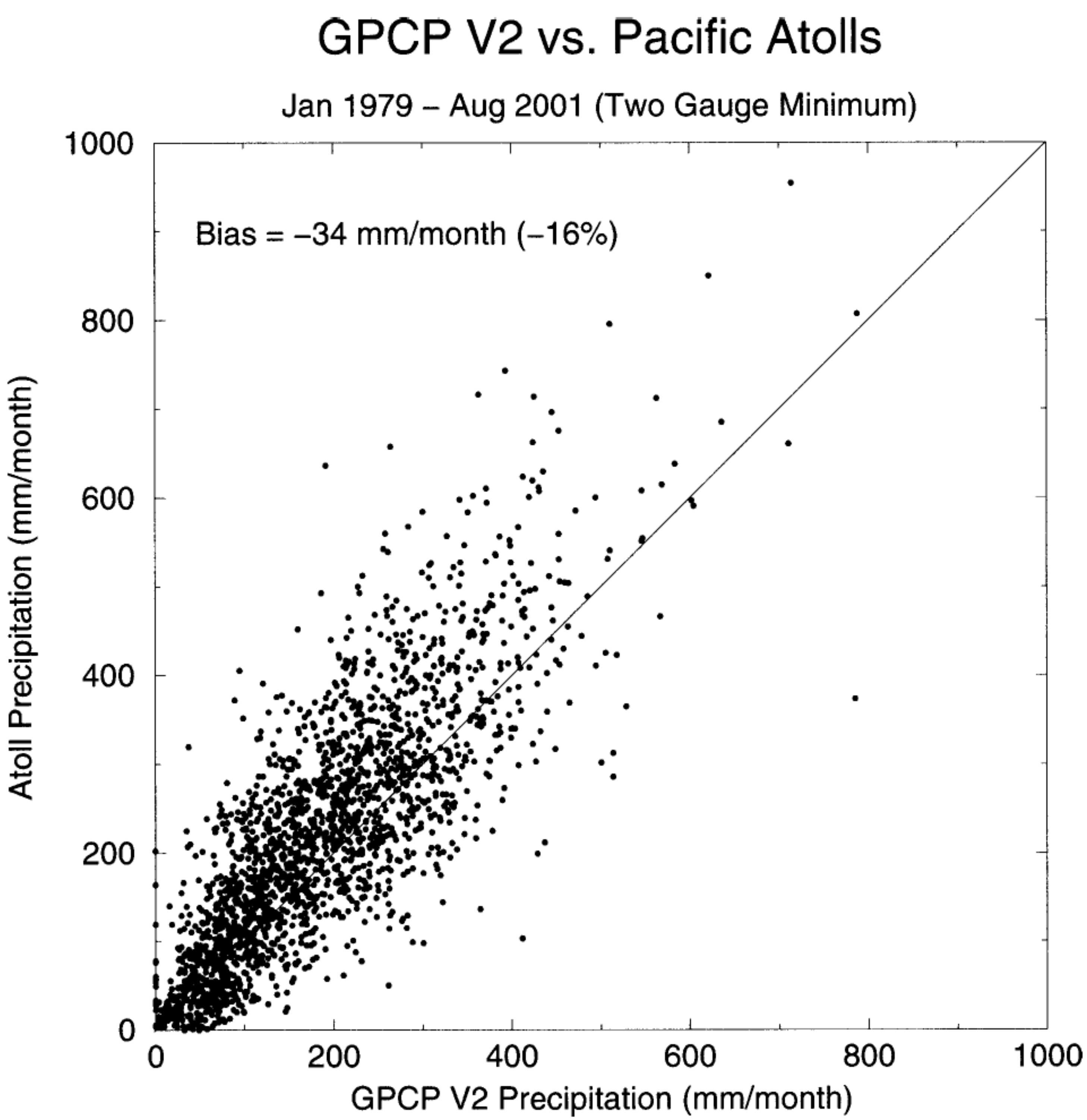

FIG. 14. Scatterplot of precipitation (mm day^{-1}) for collocated GPCP grid blocks and Pacific atoll rain gauge stations for 1979–2001.

GPCP: comparison with independent rain gauges

Fig. 18

Adler, J. Hydrometeor., 2003; fig 14

Atafu atoll; South Pacific near New Zealand

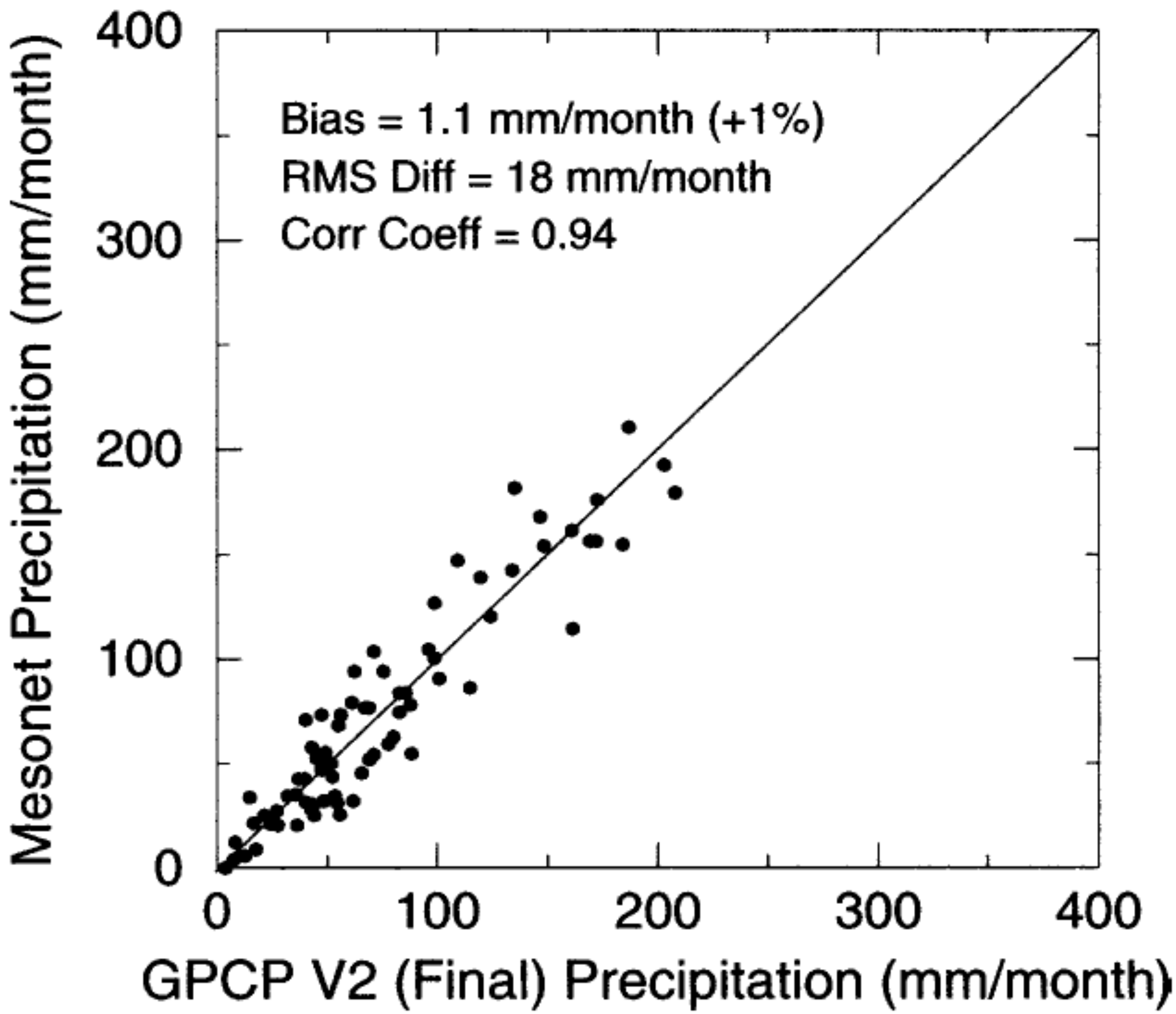

GPCP: comparison with independent rain gauges in Oklahoma

Fig. 19

Adler, J. Hydrometeor., 2003; fig 15c

Comparison of annual precipitation (mm) from different global precipitation datasets

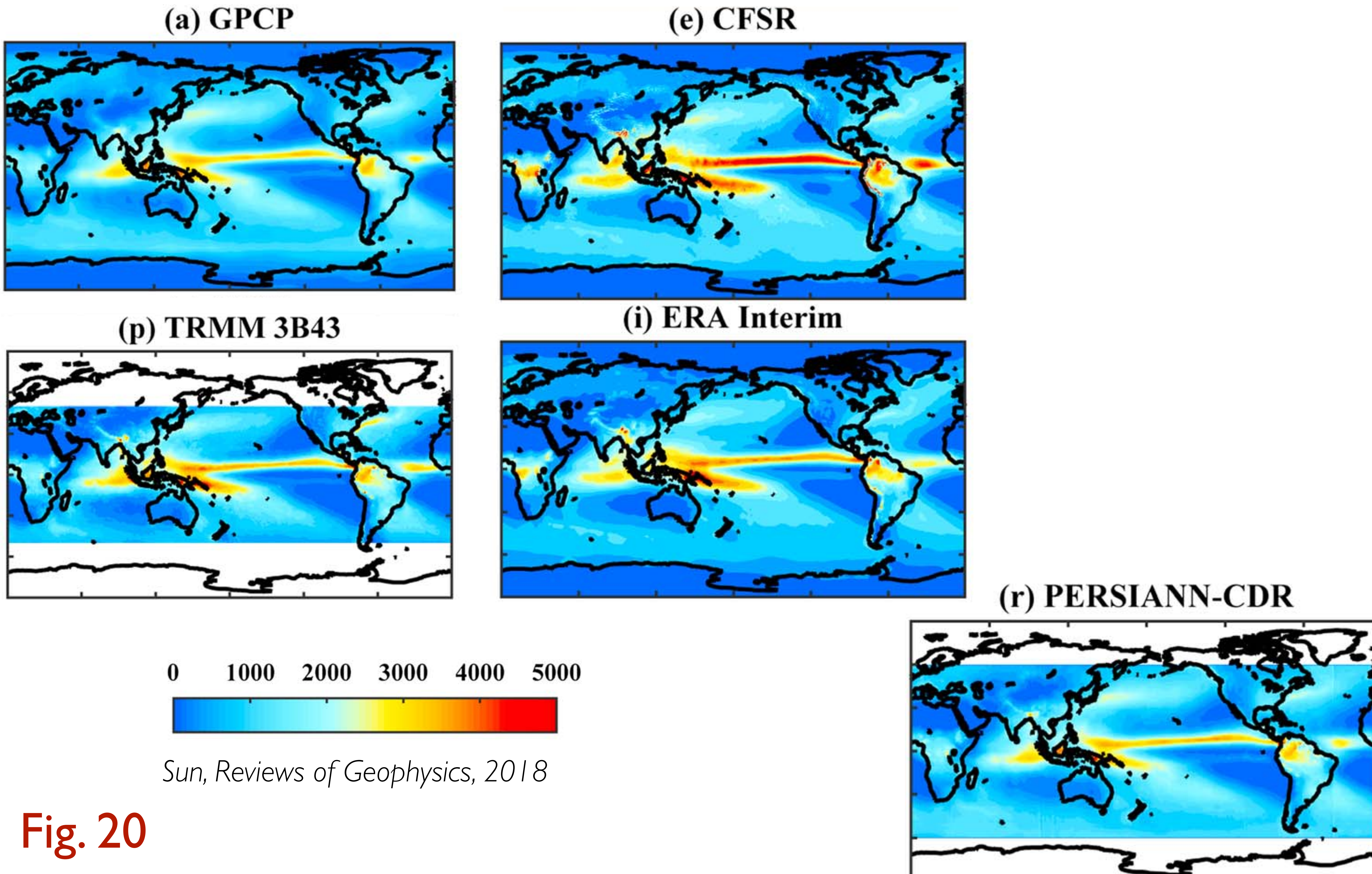

Sun, Reviews of Geophysics, 2018

Fig. 20

Surface latent heat flux (negative upwards, W/m^2)

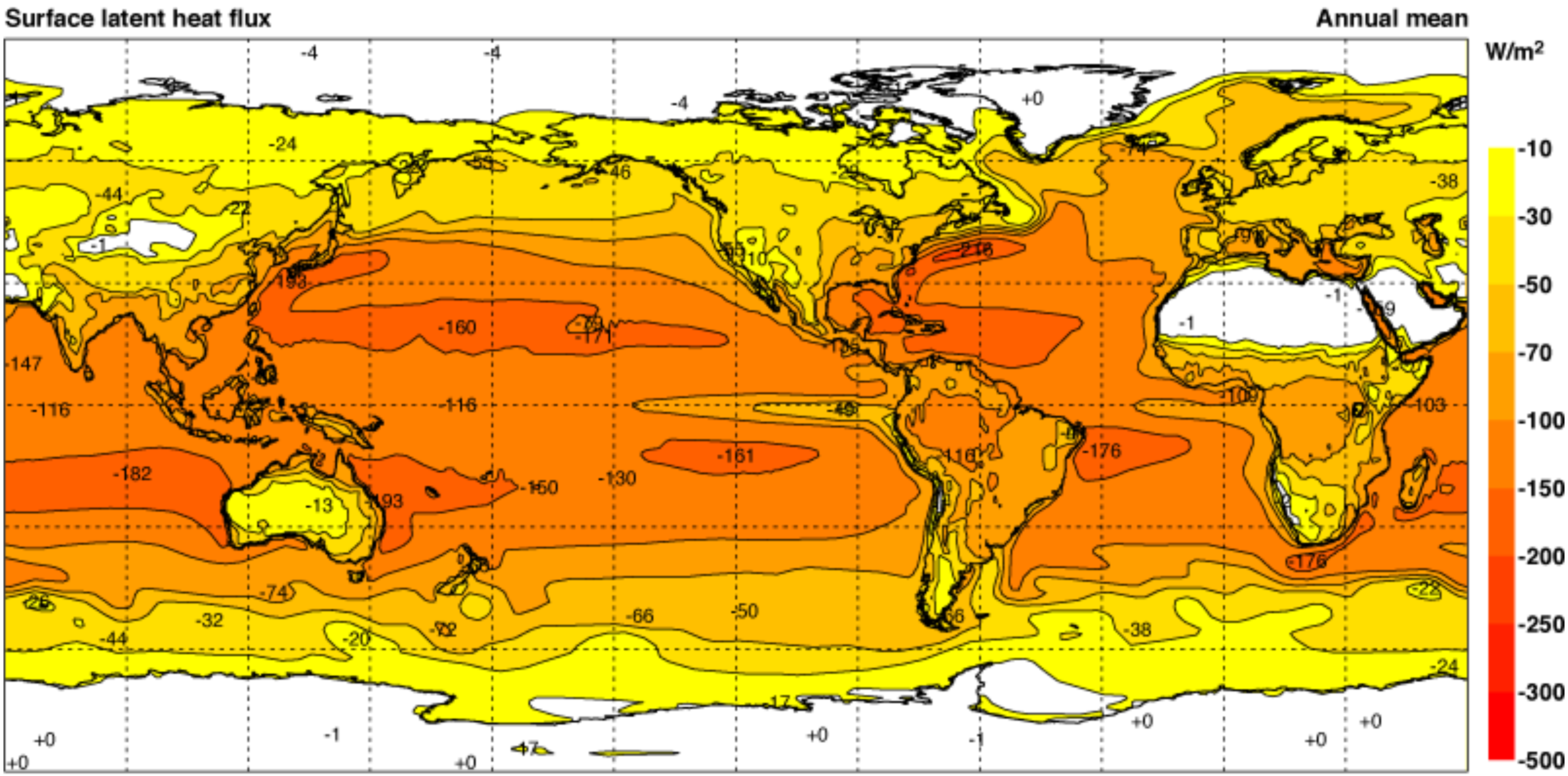

ERA40 atlas

Fig. 21

Zonal-mean evaporation rate over oceans (cm/year)

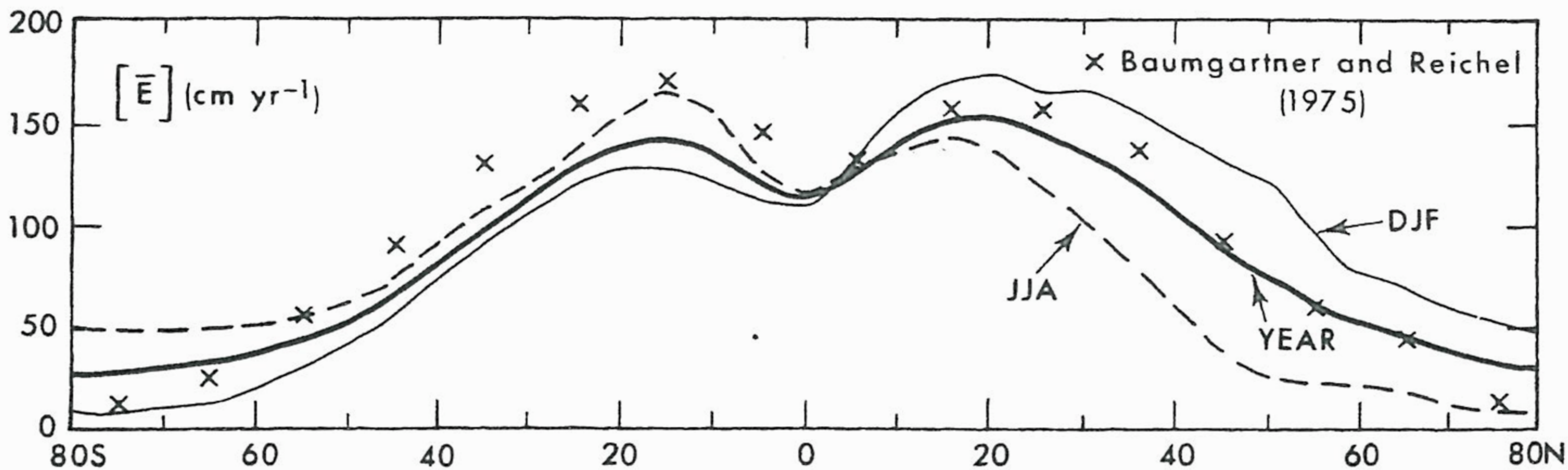

FIGURE 7.27. Meridional profiles of the zonal-mean evaporation rate (in cm yr^{-1}) over the oceans computed using Eq. (10.38) and our 1963–73 surface data. Baumgartner and Reichel's (1975) ocean values from Fig. 7.26 have been added for comparison.

Fig. 22

Peixoto and Oort, Fig 7.27

Radiative importance of upper-tropospheric water vapor

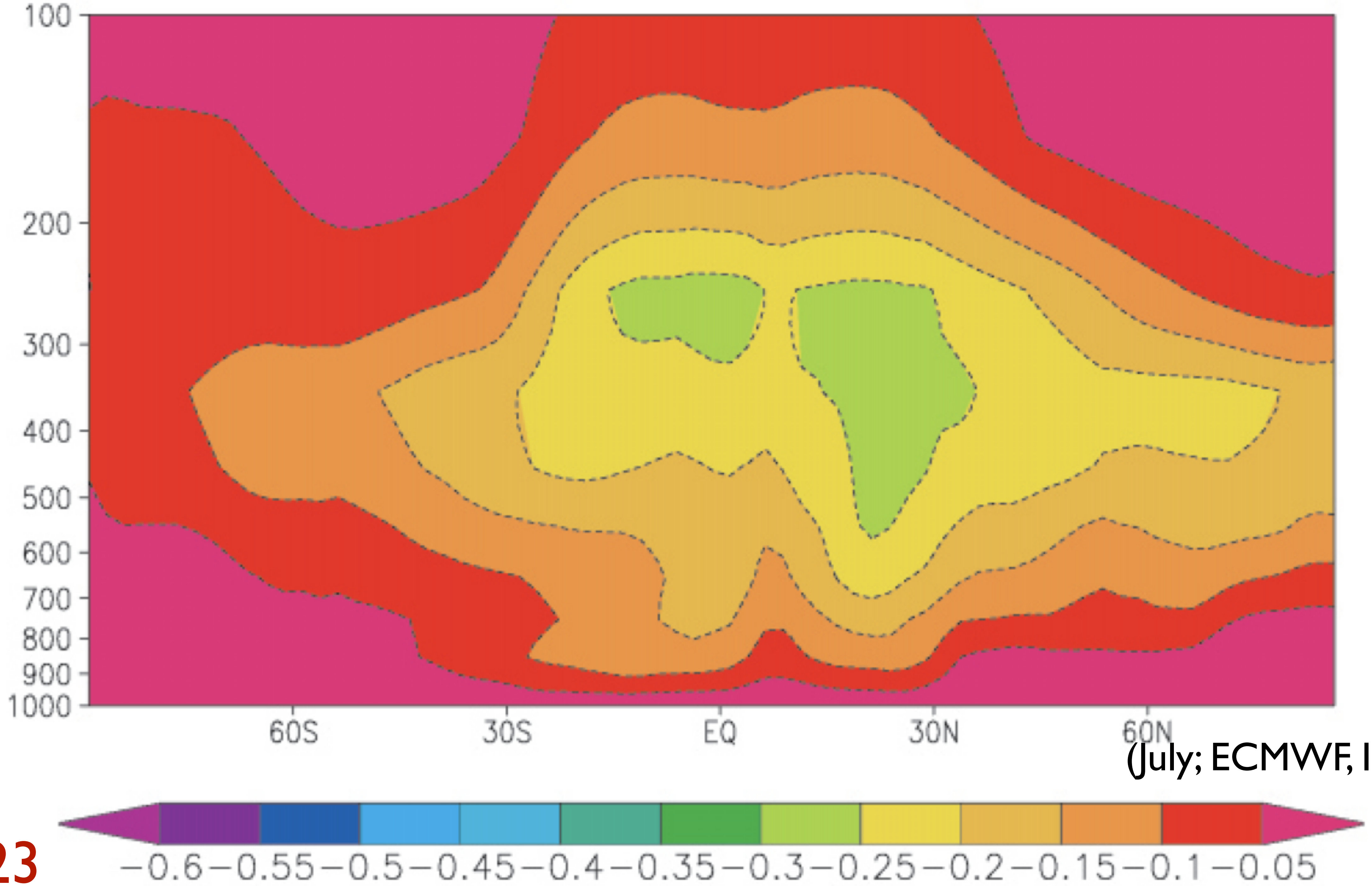

(July; ECMWF, ISCCP data)

Fig. 23

Sensitivity of outgoing longwave radiation to a change in local specific humidity (W/m^2/K). Change in specific humidity is the change that would occur at constant relative humidity for a 1K increase in temperature.

Held and Soden, 2001

Transport and mixing of water vapor in the troposphere

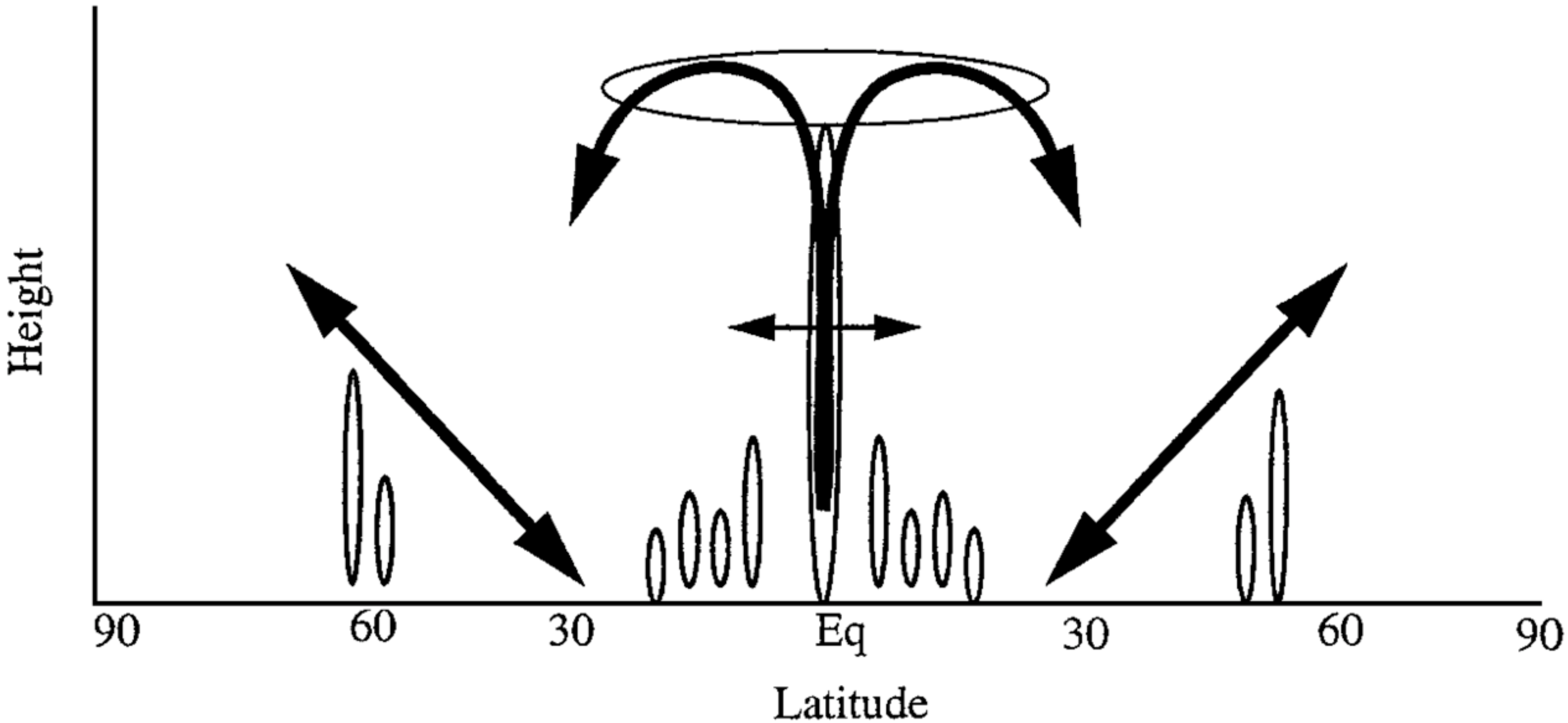

Figure 8 A height-latitude schematic of the large-scale atmospheric trajectories involved in the transport and mixing of moisture within the troposphere.

Held and Soden, 2001

Fig. 24

Potential temperature (K)

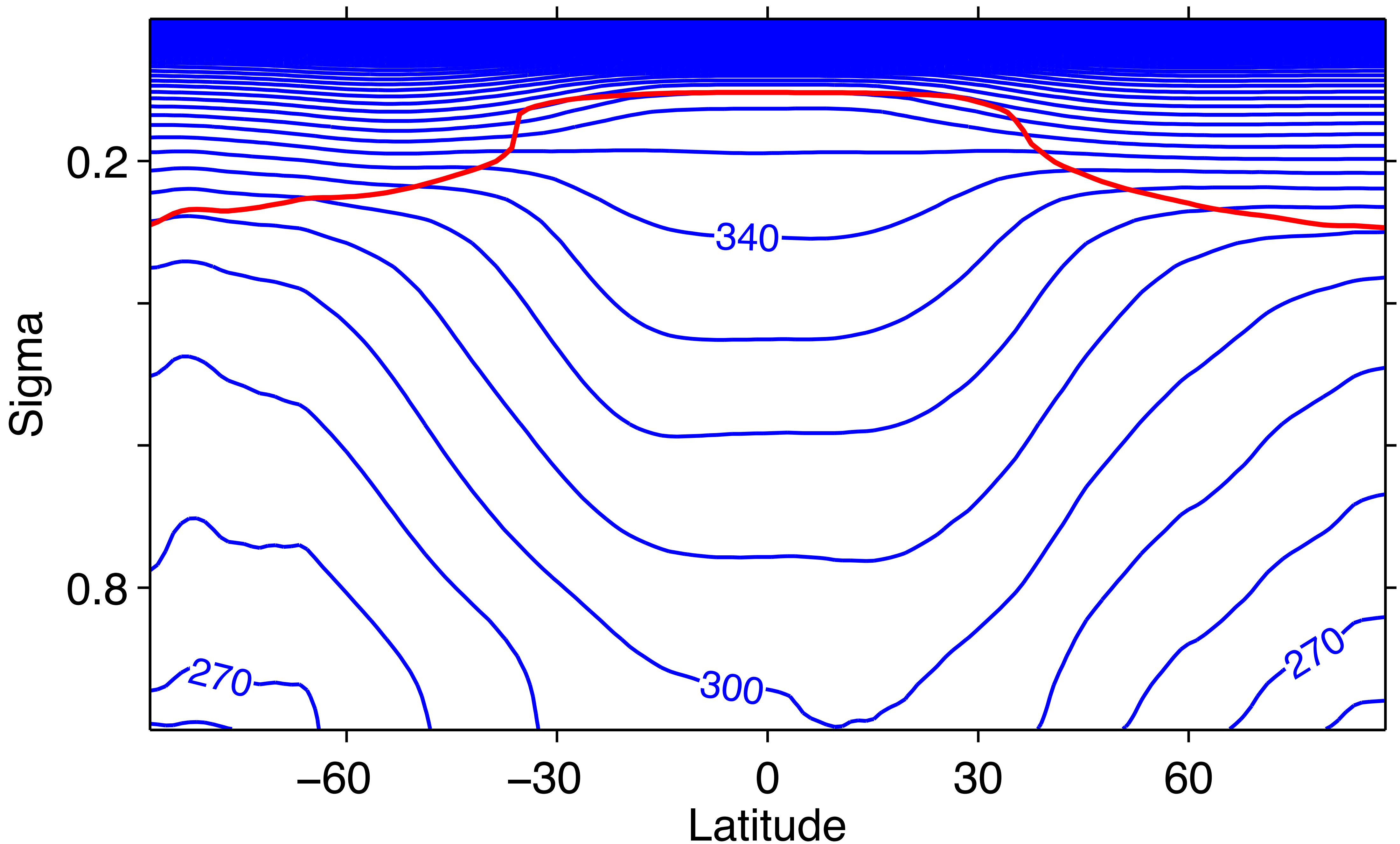

(ERA40 reanalysis data 1980-2001)

Last saturation analysis of mean relative humidity: NCEP winds and MATCH tracers

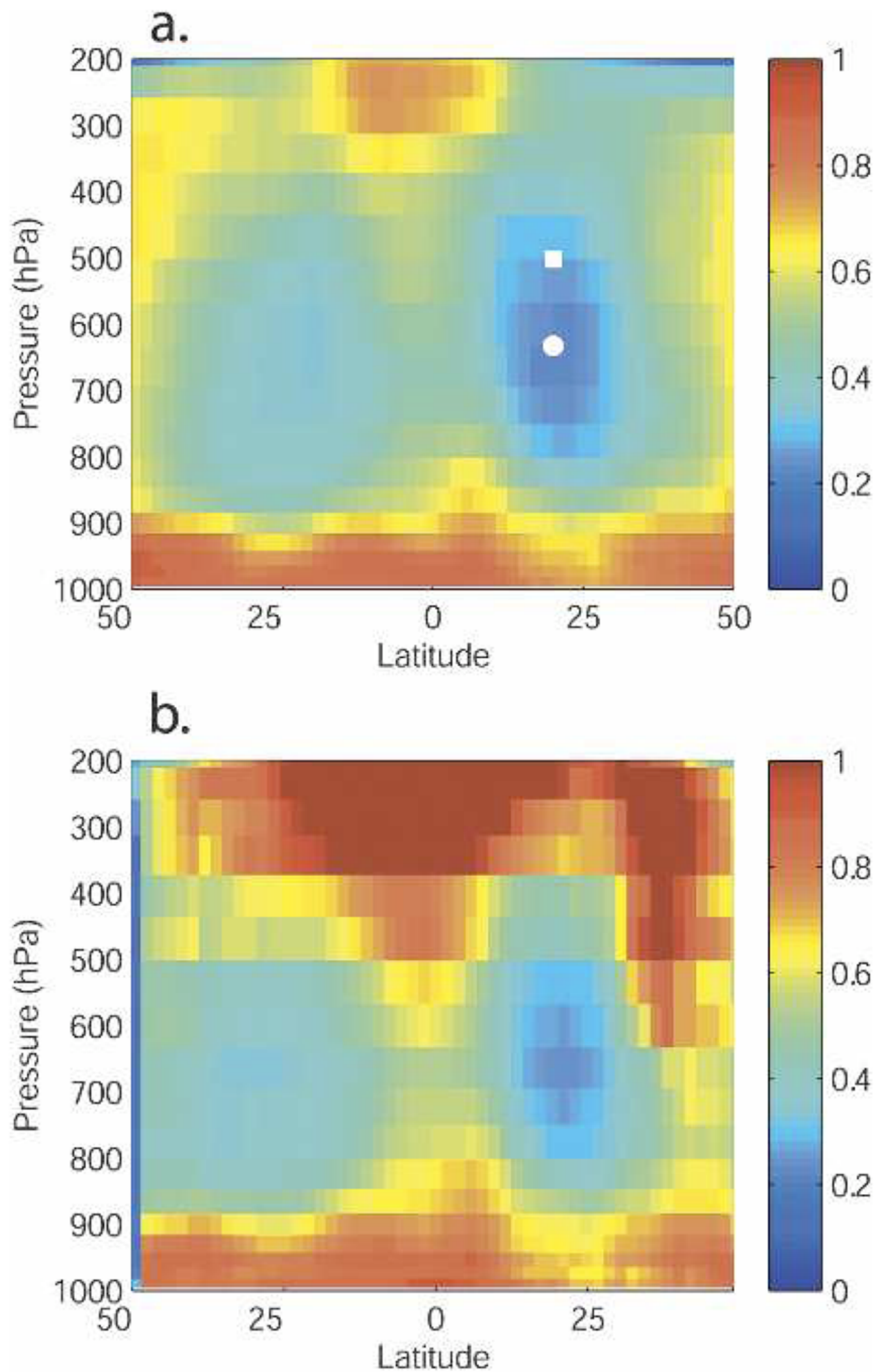

FIG. 9. DJF 2001/02 zonal-mean RH: (a) MATCH hydrologic cycle applied to NCEP–NCAR reanalysis data; (b) reconstructed from tracer calculation.

RH from NCEP/MATCH

Reconstructed RH using tracers of last saturation

Galewsky et al, JAS, 2005; fig 9

Fig. 25

PDF of last saturation

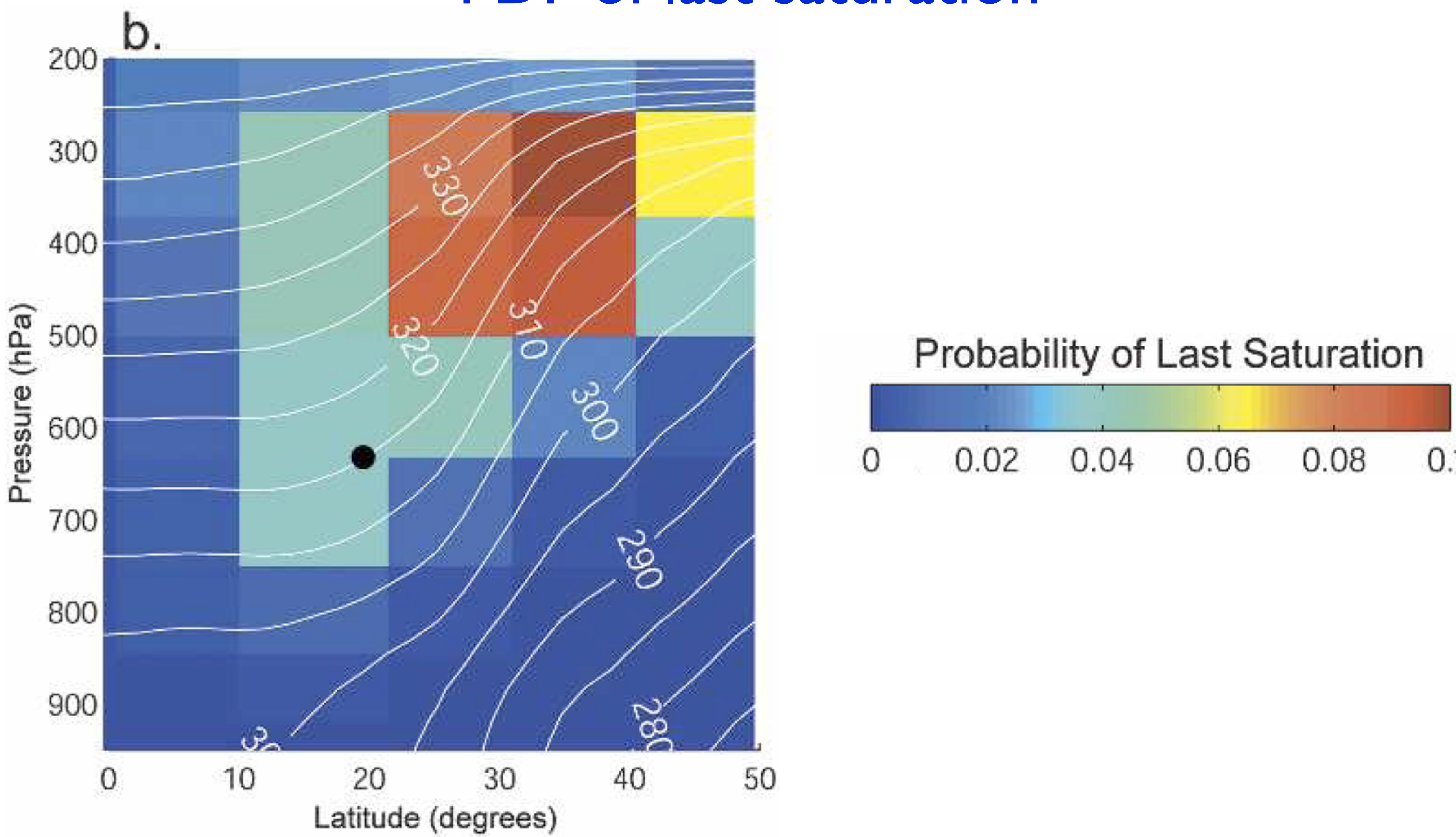

FIG. 12. Zonal-mean probability of location of last saturation for two reference points: (a) upper region of dry zone (location of point shown by white square in Fig. 9a); (b) central region of dry zone (location of point shown by white circle in Fig. 9a). Contours are potential temperature in degrees kelvin.

Galewsky et al, JAS, 2005; fig 12b

Fig. 26